



Experimental evaluation of the role of oxygen on the growth of MgO_x nano-sculpted thin films synthesized by reactive magnetron sputtering combined with glancing angle deposition

X. Geng^{a,b,1}, H. Liang^{a,b,1}, W.J. Li^{a,c}, A. Panepinto^{b,*}, D. Thiry^b, M.F. Chen^{a,c}, R. Snyders^{b,d}

^a School of Materials Science and Engineering, Tianjin University of Technology, 300384 Tianjin, China

^b Chimie des Interactions Plasma-Surface, University of Mons (Umons), 20 Place du Parc, B 7000 Mons, Belgium

^c Key Laboratory of Display Materials and Photoelectric Device (Ministry of Education), 300384 Tianjin, China

^d Materia Nova Research Center, 1 Avenue Nicolas Copernic, B 7000 Mons, Belgium

ARTICLE INFO

Keywords:

Nano-sculpted MgO_x films
Poisoning mechanism
Glancing angle deposition
Reactive magnetron sputtering

ABSTRACT

In this work, we have studied the influence of oxygen on the chemistry and morphology of nano-sculpted MgO_x thin films prepared by magnetron sputtering in glancing angle configuration. First, we have studied the poisoning mechanism of the Mg target by² combining target voltage and deposition rate measurements with chemical analysis of the deposited films by X-ray Photoelectron Spectroscopy. The results reveal a strong metal-to-compound transition at very low oxygen flows, namely < 5% of O₂ in the gas mixture. This transition is accompanied by a dramatic decrease of the deposition rate (by 95%) and by the synthesis of fully oxidized films. Then, for three gaseous mixtures corresponding to the metallic conditions as well as to the edges of the metal-to-compound transition, namely 0%, 2.5% and 5% of O₂ in the gas mixture, nano-sculpted films have been grown. From SEM images, it appears that even a slight amount of O₂ in the gas mixture strongly affects the morphological features of the films by reducing the width of the tilted columns (by 50% for 2.5% of O₂) as well as the intercolumnar space (by 85% for 2.5% of O₂). This has been understood by considering the growth mechanism of thin films in reactive conditions and the Structural Zone Model associated with these conditions.

1. Introduction

In the context of the necessary transition towards renewable energies, the use of hydrogen as a fuel is more and more considered. Indeed, hydrogen can be produced by various electrochemical and biological methods and has a higher chemical energy when compared to fossil fuels [1–3]. Considering the utilization of fuel cells, hydrogen generates electricity leaving water vapor as the only exhaust gas, without any other greenhouse gasses or harmful emissions [4]. Although the potential of hydrogen fuel associated with fuel cells utilization is a real promise for the future generations, several issues related to the production, distribution and storage of hydrogen have to be fixed before an economically viable utilization of hydrogen [5].

Specifically, because of the low volumetric density of hydrogen, the hydrogen storage is a critical issue that could be fixed by using solid state materials because of their higher volumetric density (as compared with

gaseous and liquid) and for safety reasons [6–8]. More precisely, hydride materials in which hydrogen is chemically bounded (i.e. not only adsorbed) is foreseen as promising materials and especially elemental magnesium hydride (MgH₂). Indeed, Magnesium (Mg) is abundant and low cost and has a light density, a low toxicity, a high gravimetric, a high hydrogen capacity and a higher reversibility in comparison with other hydrides [9,10]. Nevertheless, this compound suffers of two main drawbacks which are a high desorption temperature and a slow hydrogen sorption kinetic. In addition, (i) Mg can easily be oxidized by oxygen and air and (ii) hydrogen not easily diffuse in bulk Mg [10,11].

Since many years these problems have been addressed by the community by using catalysts and reduction of the particle size to rectify the thermodynamic barriers and to improve the sorption kinetic [5,9,12,13]. In this context, we have recently reported on an innovative synthesis road allowing for the controlled design of nano-sculpted Mg thin films by using Magnetron sputtering (MS) and Glancing Angle

* Corresponding authors.

E-mail address: adriano.panepinto@umons.ac.be (A. Panepinto).

¹ XG and HL have contributed to the paper equally. They both should appear as first authors.

Deposition (GLAD) [14]. In this work, we have shown that it is possible to finely tune the Mg nano-sculpted films features by adapting the deposition parameters such as deposition angle, working pressure... Nevertheless, we also have observed that the presence of oxygen, even in the form of traces during the deposition procedure (which is often the case in vacuum systems) strongly affects the features of the deposited coatings. This effect is not yet understood neither controlled therefore making necessary a dedicated study.

In the present work, we therefore aim to study the growth of nano-sculpted MgO_x films by combining reactive magnetron sputtering and glancing angle deposition (MSGLAD) in order to better understand the role of oxidation on the morphology of the deposited nano-sculpted films. First, we study the poisoning mechanism of the Mg target by combining target voltage, and deposition rate measurements with chemical analysis by X-ray Photoelectron Spectroscopy (XPS). These measurements have been performed in conventional geometry, producing dense crystallized films. Then, for three gaseous mixtures corresponding to the metallic conditions as well as to the edges of the transition, namely 0%, 2.5% et 5% of O_2 , nano-sculpted films have been grown in order to evaluate the impact of the gas mixture on the morphological features of the films. The data have been understood by considering a Structural Zone Model associated with the different growth conditions.

2. Material and method

All experiments were carried out in a cylindrical stainless steel chamber (height: 60 cm, diameter: 42 cm), see Fig. 1. The chamber was evacuated by a turbo-molecular pump (Edwards nEXT400D 160 W), down to a residual pressure of 10^{-7} Pa. A magnetron cathode was installed at the top of the chamber and the substrate is located at a distance of 80 mm. A 2-inch in diameter and 0.25-inch thick Mg target (99.99% purity) was used. The target was sputtered in DC mode using an Advanced Energy MDK 1.5 K power supply in Argon (12 sccm) or in argon/oxygen gas mixtures. In the latter case, the total flow is constant (12 sccm) while the Ar and oxygen flows were varied from 12 to 0 sccm, respectively. We therefore defined the content of oxygen in the gas mixtures (% O_2) as the ratio between the oxygen flow and the total flow.

Conductive silicon wafers (100) were used as substrates, and rinsed

with ultra-pure water before deposition.

Using a GLAD-adapted substrate holder, the substrate can be tilted with an angle α and eventually rotated by an angle (φ) either step by step or with a continuous angular speed in order to generate diverse thin films architectures. In this work, we have fixed the tilt angle at 85° ($\alpha = 85^\circ$) and the working pressure (P_{tot}) at 0.26 Pa. This choice is made based on our previous work in which these experimental conditions have been determined to allow for an important porosity of the deposited films [14]. For all depositions, the sputtering power was kept constant at 50 W and the deposition time was 20 min. The discharge voltage (V_D) as well as the deposition rate (R_D) have been measured as a function of the oxygen flow for $\alpha = 0^\circ$ while the other experimental parameters have been kept constant.

The morphology of the material was characterized with a field emission gun scanning electron microscope (FEG-SEM, Hitachi SU8020).

The chemical composition of the films was evaluated by X-ray Photoelectron Spectroscopy (XPS) on a VERSAPROBE PHI 5000 hemispherical analyzer from Physical Electronics with a base pressure of $< 3 \times 10^{-7}$ Pa. The X-ray photoelectron spectra were collected at the take-off angle of 45° with respect to the electron energy analyzer, operating in constant analyzer energy mode (23.50 eV). The spectra were recorded with the monochromatic Al K_α radiation (15 kV, 25 W) with a highly focused beam size of 100 μm . The energy resolution was 0.7 eV. The binding energy scale of the spectra was calibrated with respect to the aliphatic component of the C1s peak at 285 eV. Eventual surface charging was compensated for by a built-in electron gun and an argon ion neutralizer. For the chemical depth profile, an Ar^+ ion source was operated at 1 μA and 2 kV with a raster area of 2 mm \times 2 mm at an incident angle normal to the sample surface of 54.7° . The XPS spectra were referenced to the Mg2p peak at 49.5 eV arising from the metallic magnesium component [15]. Atomic compositions were derived from peak areas using photoionization cross sections calculated by Scofield, corrected for the dependence of the escape depth on the kinetic energy of the electrons.

The thickness of the films, as measured by a mechanical profilometer Dektak 150 from Veeco, was kept constant for all films (700 ± 50 nm).

Finally, the phase constitution of the samples was evaluated by X-ray diffraction (XRD) using a PANalytical Empyrean diffractometer working with Cu $K_{\alpha 1}$ radiation ($\lambda = 0.1546$ nm) in the grazing incidence configuration ($\Omega = 0.5^\circ$). The X-ray source voltage was fixed at 45 kV and the current at 40 mA. The grain size (G_s) was calculated from the XRD pattern using the following Scherrer equation [16]:

$$G_s = \frac{K \lambda}{\beta \cos \theta}$$

where K is a dimensionless shape factor, λ is the X-ray wavelength, β is the diffraction line broadening at half the maximum intensity and θ is the Bragg angle.

3. Results and discussion

3.1. Study of the target poisoning

In order to ultimately evaluate the impact of the oxidation of Mg on the features of MSGLAD deposited thin films, it is decided to synthesize nano-sculpted MgO_x films in reactive mode. In this context, we first have evaluated the Mg target poisoning mechanism when adding O_2 to the sputtering process. This study is performed using a conventional deposition geometry ($\alpha = 0^\circ$) and for fixed sputtering power and working pressure of 50 W and 0.26 Pa, respectively.

For these conditions, the target voltage (V_D) and the deposition rate (R_D) of the films which are known to be good indicators of the target poisoning have been measured as a function of % O_2 (Fig. 2). Our measurements reveal that, as expected and because of its reactivity for O_2

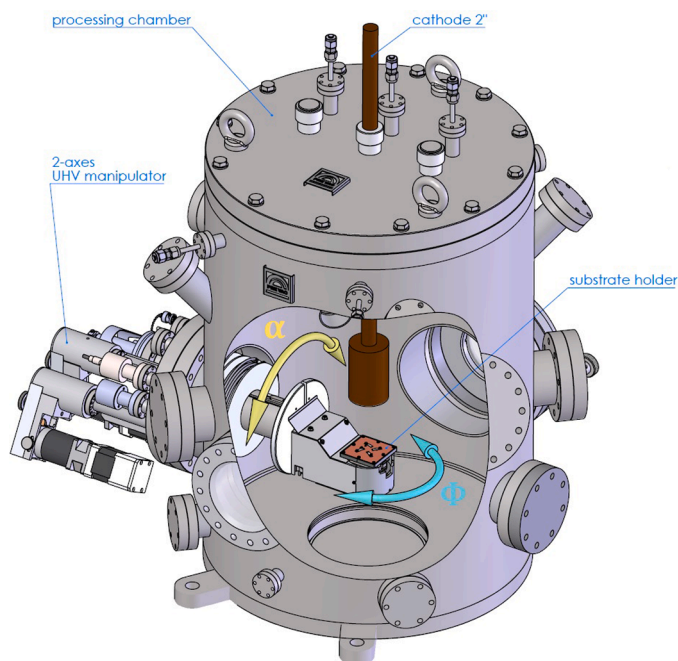


Fig. 1. Sketch of the deposition chamber used in this work.

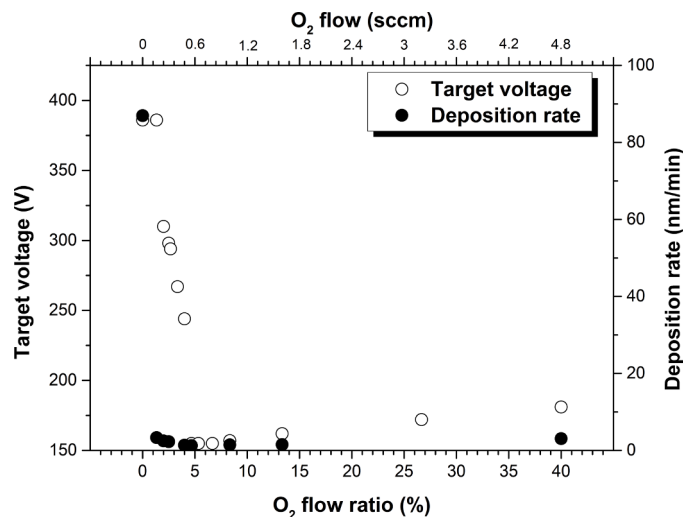


Fig. 2. Evolution of the target voltage (V_D) and the deposition rate (R_D) of the MgOx films as a function of $\%O_2$. The deposition conditions are $\alpha = 0^\circ$, sputtering power and working pressure of 50 W and 0.26 Pa, respectively.

demonstrated by the elevated enthalpy of formation for MgO compound ($\Delta H_{f(MgO)} = -601.8 \text{ kJ}\cdot\text{mol}^{-1}$) [17], the target is poisoned for very low O_2 flows (0.5–1 sccm, corresponding to 4–8% O_2 in the gas mixture). This is deduced from the strong decrease of both V_D (Fig. 2a) and R_D (Fig. 2b) for this O_2 flow range. This $\%O_2$ is therefore defined as the critical content for which the target transits from its “metallic mode” to its “poisoned mode”. As already reported for Mg [18], and other materials [19], it is well known that this transition occurs when the target surface is covered by the oxidized compound, namely MgO_x in our case. The mechanism of formation of this oxide layer has been described in detail by several groups and is related to the implantation of reactive ions in the target [19,20].

When this covering occurs, in the case of the Mg target, the secondary electron emission yield increases leading to the observed decrease of V_D [19]. On the other hand, because of this decrease of V_D as well as because of the lower sputtering yield of MgO_x when compared to Mg, R_D decreases dramatically for the same value of the O_2 flow. For $\%O_2 > \sim 5\%$, meaning after the transition, we observe a slight increase of V_D that is associated to the modification of the gas mixture which contains more and more oxygen. This phenomenon has already been explained in details in [20]. As a consequence, R_D also slightly increases for these conditions. From these data, it can be expected that a very small amount of O_2 in the gas mixture leads to the formation of a fully oxidized film.

In order to validate this hypothesis, two “reference” films have been grown using a conventional deposition geometry ($\alpha = 0^\circ$ and $P_{tot} = 0.26$ Pa) for $\%O_2 = 0\%$ (Sample 1) and $\%O_2 = 5\%$ (Sample 2) using a sputtering power of 50 W in each case. Sample 1 is expected to correspond to a fully metallic Mg film since it is prepared in the “metallic mode” of the target (for $\%O_2 < \text{critical}\%O_2$) while Sample 2 is grown for gaseous conditions corresponding to the “poisoned mode” (for $\%O_2 > \text{critical}\%O_2$) and therefore should correspond to a stoichiometric MgO film. The chemistry of these coatings has been analyzed by XPS. The XPS survey spectra of both samples are presented in Fig. 3. On these spectra, we observe the presence of Mg, O and C atoms on the surface of both samples even if, for Sample 1, the coating has been prepared without oxygen in the sputtering atmosphere.

Table 1 reports the XPS quantification of these elements for as-prepared Samples 1 and 2. From these data we learn that the surface composition is similar for both samples. A first observation is that the presence of carbon, which is associated to surface contamination by atmospheric hydrocarbons during the transfer of the samples from the preparation chamber to the XPS machine, is observed for both samples. On the other hand, oxygen is also present on both surfaces. This is

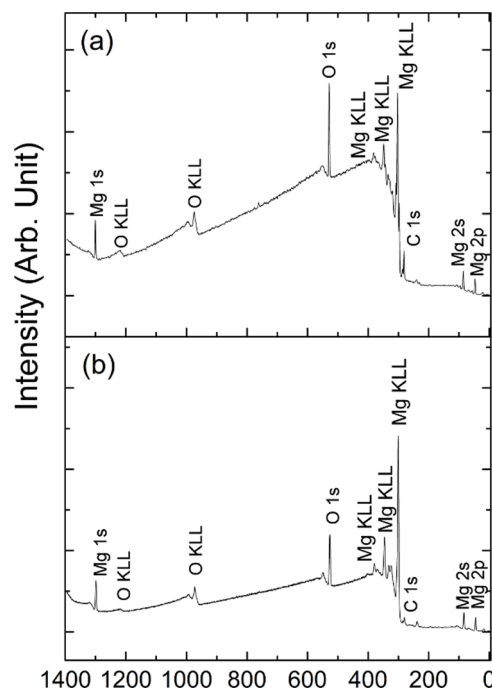


Fig. 3. XPS survey spectra of (a) Sample 1 prepared for $\%O_2 = 0$, $\alpha = 0^\circ$ and $P_{tot} = 0.26$ Pa; (b) Sample 2 prepared for $\%O_2 = 5\%$, $\alpha = 0^\circ$ and $P_{tot} = 0.26$ Pa.

Table 1

Elemental composition of Samples 1 and 2 evaluated by XPS before and after 2 min of erosion.

	At.% Mg		At.% O		At.% C	
	As prepared	After erosion	As prepared	After erosion	As prepared	After erosion
Sample 1	41	90	49	10	10	0
Sample 2	45	48	49	52	6	0

expected for Sample 2 prepared in reactive conditions while, for Sample 1, it is associated with an oxidation reaction which likely occurs during the transport of the sample to the XPS machine as already considered to explain the presence of carbon. Nevertheless, we should also consider that this reaction could also occur during the synthesis of the films taken into account that even if a good quality base vacuum of 1.33×10^{-5} Pa is measured, the base partial pressure of oxygen or water vapor in the sputtering chamber is not 0 allowing for a reaction with the sputtered metal.

In order to clarify the chemistry of both films and to validate that, for Sample 1, the presence of carbon as well as the surface oxidation of Mg is (or not) occurring during the synthesis of the films, both samples have been depth profiled in the XPS machine. XPS spectra have been recorded after 0 (as prepared), 2, 4 and 20 min of erosion. The estimated sputtering rate is ~ 20 nm/min, according to the study reported by Milcius et al. [21]. Fig. 4 shows the evolution of the Mg XPS line as a function of depth for Sample 1 and Sample 2. For the as-deposited Sample 1 (Fig. 4a), it appears that the Mg line is mainly composed by two components likely corresponding to metallic Mg at 49.5 eV and MgO at 50.8 eV [22]. A tiny third component at a binding energy of ~ 52 eV associated with $Mg(OH)_2$ species is also necessary to ideally fit the XPS peak. This is consistent with the report of Fuggle et al. which demonstrates by XPS that, in the presence of water vapor and oxygen, magnesium films easily form a top-surface oxide layer containing significant amounts of hydroxyl or hydroxide species [23]. In addition to this main peak, a broad peak centered at ~ 60 eV which is associated to a satellite

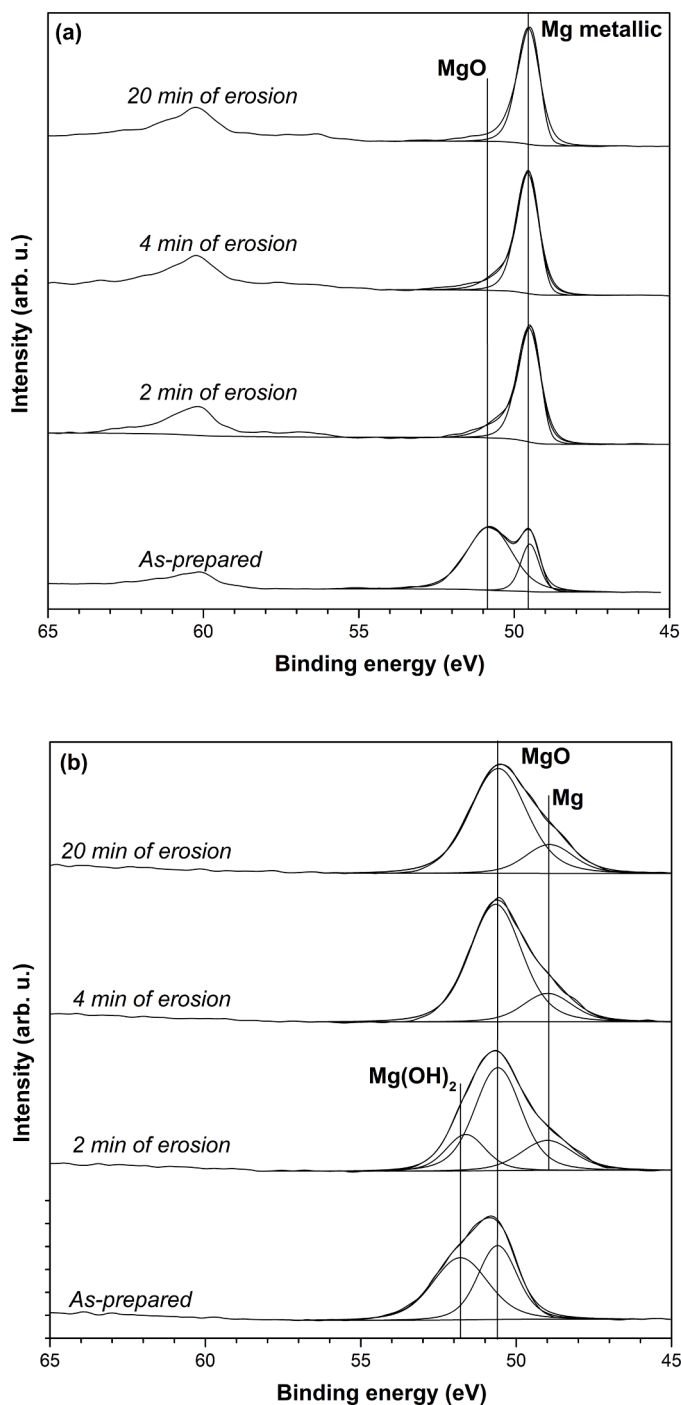


Fig. 4. Evolution of the Mg2p lines during the depth profiling of the Mg films prepared for $\alpha = 0^\circ$ and $P_{\text{tot}} = 0.26$ Pa: a) for $\%O_2 = 0\%$ and (b) for $\%O_2 = 5\%$. The sputtering power is 50 W.

contribution of metallic Mg is observed as well. This peak is specific of the metallic character of the material [24]. The presence of a strong oxidized component on the surface of the as-deposited Sample 1 is in line with the surface composition from Table 1. After a few minutes (2–3 min) of erosion which is evaluated to correspond to the generation of a 40 nm in depth crater, the XPS spectrum is strongly modified. Indeed, the oxidized/hydroxyl component of the Mg peak completely vanishes and the satellite component is more evident. This suggests that Sample 1, prepared in non-reactive conditions, is oxidized on its top surface mainly while being much more metallic in its bulk. This is again in line with the composition of the films which reveals that after this 2–3

min of erosion, the oxygen content drops until a maximum of $\sim 10\%$ in the bulk of the film. Simultaneously, the carbon completely disappears as expected (Table 1). Further erosion duration does not impact significantly the feature of the Mg2p line meaning that a stable chemical composition is reached. The presence of the 10 at.% of oxygen in the bulk of the material is likely explained by the presence of residual water vapor or oxygen in the deposition chamber even if the base pressure is of good quality (1.33×10^{-5} Pa). Indeed, because of the already mentioned strong reactivity of Mg towards oxygen, a getter effect likely occurs leading to the partial oxidation of the material similarly as the effect already observed for other getter materials such as Ti [25].

For Sample 2, the as-deposited surface analysis reveals that both MgO and Mg(OH)₂ species are present on the surface as well. Nevertheless, we do not observe any satellite peak which is consistent with the supposed oxidized character of the material. After 2 min of erosion (~ 40 nm depth), the Mg2p peak is strongly modified because of the strong reduction of the Mg(OH)₂ component and of the appearance of the metallic Mg component at lower binding energy. The disappearance of the hydroxyl signal reveals that it is mostly present on the sample surface. On the other hand, the appearance of the metallic component could be explained by an incomplete oxidation of the film in its bulk and/or by the ion erosion process which, considering the sputtering yield of the elements, generates a modification of the material chemistry because of a preferential sputtering of oxygen vs magnesium. Such a phenomenon is often observed during the depth profiling of oxides [26], and is confirmed by TRIDYN which simulates sputtering yields of 1.73 and 2.03 atoms/ions for Mg and O atoms, respectively, in the used sputtering conditions. When increasing the erosion duration, the hydroxyl contribution vanishes while the relative intensities of the Mg²⁺ and Mg⁰ line stabilize.

Based on the data, we can conclude that the bulk of the Mg film synthesized in metallic condition ($\%O_2 = 0$) only contains a low level of oxygen which should not be detrimental in view of the foreseen application for hydrogen storage. Nevertheless, an oxide/hydroxide layer is formed on the top of the film because of the venting of the sample and of the strong reactivity of Mg towards oxygen and water vapor. This layer could be avoided if the metallic Mg film is protected before venting by a selective gas barrier layer allowing the diffusion of H₂ but avoiding the one of O₂. The development of such material architecture is foreseen in our project but is obviously out of the scope of the present work.

In order to get a complete understanding of the material structure, the phase constitution of our reference films has been evaluated by XRD measurements. The XRD analysis of the as-deposited films (1 and 2) are presented in Fig. 5. The diffractograms reveal that both coatings are crystallized with the presence of several diffraction peaks for both samples that are attributed to the cubic phase of Mg (JCPDS card N° 04-0770) for Sample 1 and to the cubic (JCPDS card N° 70-9183) and hexagonal (JCPDS card N° 77-8619) phases of MgO for Sample 2. These data support the metallic character of Sample 1 although a slight quantity of oxygen is present in the film (< 10 at.%). It has to be mentioned that for sample 2, a tiny peak attributable to metallic Mg can also be observed which likely confirms that the bulk of the film is not completely oxidized when using 5% of oxygen in the gas mixtures.

3.2. Study of the influence of the oxidation on the architecture of the nano-sculpted films

Since it is accepted that the H₂ absorption and desorption properties are related to the features at the nano-scale of the Mg material, this part of the work aims to clarify the impact of the oxidation of the material on the generated morphology. Therefore, using reactive magnetron sputtering in GLAD configuration, we have studied the influence of the addition of O₂ during the growth of the nano-sculpted films on their morphology. Based on our study of the poisoning mechanism of the target (see part 3.1), we have synthesized three samples for $\alpha = 85^\circ$, $P_{\text{tot}} = 0.26$ Pa (defined as the ideal conditions to generate high porosity

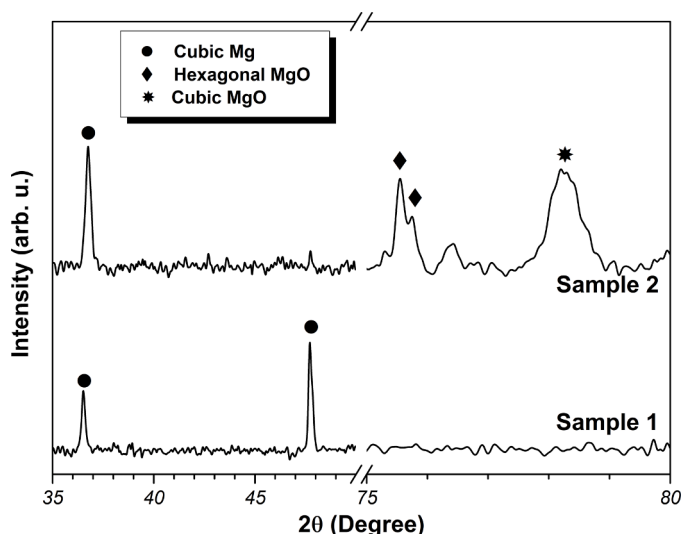


Fig. 5. XRD data of reference Sample 1 and Sample 2 prepared for $\alpha = 0^\circ$ and $P_{tot} = 0.26$ Pa and for $\%O_2 = 0\%$ and 5% , respectively. The sputtering power is 50 W.

sample in [14]) and for $\%O_2 = 0\%$, 2.5% and 5% corresponding to a “metallic” films and to thin films prepared at the edges of the metal-to-compound transition (see Fig. 2). Fig. 6 shows the evolution of the morphology of the films measured by cross-sectional SEM for the nano-sculpted samples prepared for $\%O_2 = 0$, 2.5 and 5% . These coatings

are 600, 750 and 700 nm thick, respectively.

When working in non-reactive conditions, a columnar and porous structure is observed which is consistent with the one reported in our previous work. The appearance of such a kind of structure is explained by the well-documented combination of shadowing effect and diffusion phenomenon in MSGLAD geometry [14]. It appears that the morphology of the sample is strongly affected by the addition of O_2 in the gas mixture. Indeed, although a porous tilted columnar structure is observed for all conditions, the features of these structures strongly evolve with the presence of oxygen in the plasma. Indeed, the column width and the intercolumnar space are strongly reduced when increasing $\%O_2$ as summarized in Table 2. The only stable feature is the tilt angle value, β , which is only slightly influenced by $\%O_2$. In addition, it also appears that the shape of the single column is affected as well by the oxygen content. Indeed, if the column corresponding to metallic Mg film ($\%O_2 = 0\%$, Fig. 6a) are strongly faceted, they become smoother for the samples prepared for $\%O_2 = 2.5\%$ (Fig. 6b) and for $\%O_2 = 5\%$ (Fig. 6c). These results are well supported by the top surface SEM images shown on

Table 2

Evolution of the nanostructured MgO_x films feature as a function of the O_2 content in the gas mixture. The sample are prepared for $\alpha = 85^\circ$, $P_{tot} = 0.26$ Pa and a sputtering power of 50 W.

	$\%O_2 = 0\%$	$\%O_2 = 2.5\%$	$\%O_2 = 5\%$
Tilt angle, β ($^\circ$)	$22 \pm 1.0^\circ$	$22 \pm 1.0^\circ$	$21 \pm 1.0^\circ$
Width of the column (nm)	171 ± 18	76 ± 18	56 ± 11
Inter-columnar space (nm)	120 ± 25	54 ± 32	37 ± 16

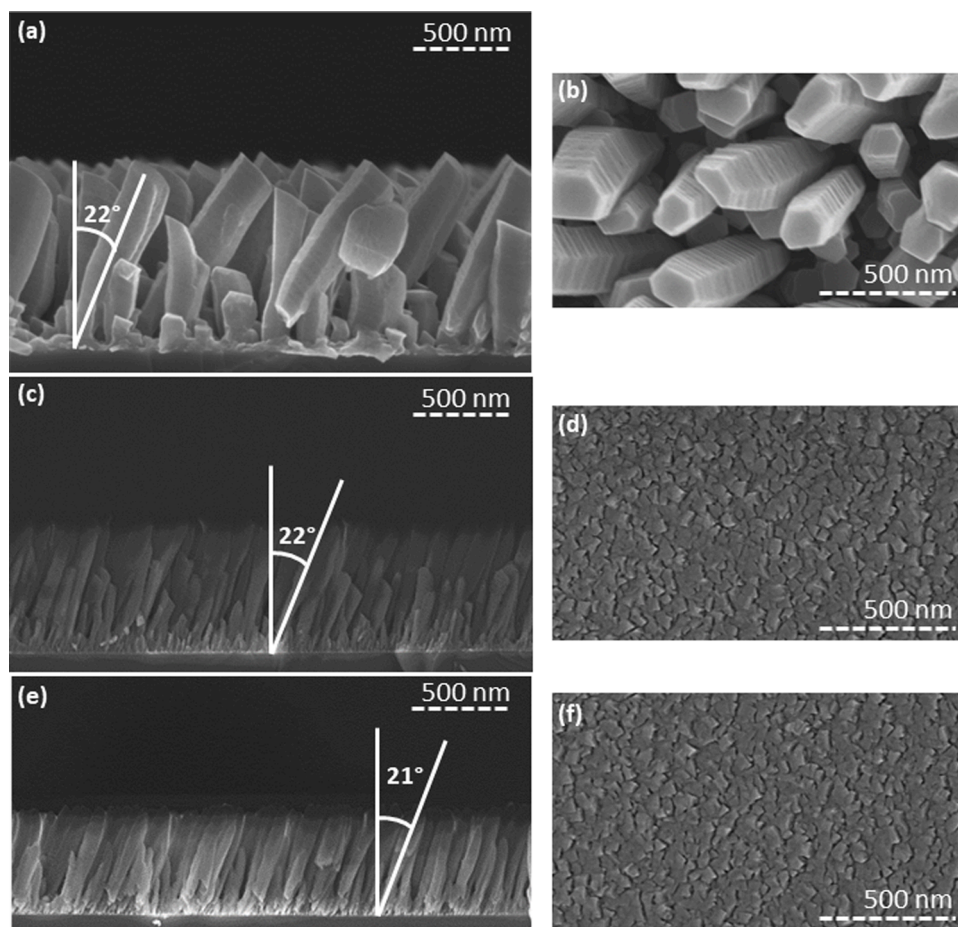


Fig. 6. Cross-section and surface SEM images evolution of the nano-architecture of MgO_x deposited films growth for $\alpha = 85^\circ$, $P_{tot} = 0.26$ Pa and for $\%O_2 = 0\%$ (a-b), 2.5% (c-d) and 5% (e-f). The sputtering power is 50 W.

Figs. 6b, d and f. Indeed, metallic Mg films are characterized by well separated columns while the oxidized films present a significantly denser structure without space between columns. It is therefore concluded that, even a low content of O_2 in the sputtering gas, can strongly affect the surface-to-volume ratio of the prepared surfaces.

These observations can be understood by considering the growth mechanism of nano-sculpted Mg thin films that has been established in our previous work [14]. In a few words, we have shown that, for metallic Mg nano-sculpted coatings, the generated architectures were mainly the results of the shadowing effect during the growth associated to a low surface diffusion of the condensing atoms. Considering this mechanism, the initially deposited atoms form small atoms assemblies on the surface that act as initial clusters on which single column are grown. In addition, these initial clusters also act as shadowing structures generating the porous structures. The density of these clusters, which is defined by diffusion phenomenon on the surface during the initial step of the growth and the subsequent coarsening of the initial grains, is therefore supposed to define the features of the deposited films (density of column, inter-columnar space, ...). And yet, considering the addition of O_2 in the system, we have demonstrated (part 3.1) that the chemistry of the material is strongly affected resulting in the presence of a MgO_x covered material even for very low value of O_2 . In addition, this growth occurs at very low deposition rate in comparison to the one of metallic Mg (19.2 nm/min vs 8.94 nm/min for the $\text{O}_2 = 2.5\%$ prepared samples). In these conditions, considering the covering of the initial clusters by an oxide layer, we expect a significant modification of the growth mechanism of the porous films since it has been demonstrated by Petrov et al. that, during the deposition of polycrystalline AlO_x thin films, the variation of the Al/O arrival rate ratio significantly impacts the film microstructure by reducing the grain coarsening [27]. A similar effect can be anticipated when considering the growth of the initial clusters on the surface in our system. In addition, the modification of the chemistry of the deposited material likely also impacts the diffusion kinetic on the growing material surface as summarized considering the Structural Zone Model approach [28]. Indeed, assuming, in a first approach, that the deposited material is MgO, the generalized temperature T^* , which is the ratio between the growth temperature (\sim room temperature) and the melting temperature of the material, becomes ~ 0.1 (vs 0.25 for metallic Mg) which means that the films microstructure mostly belongs to the Zone I of the diagram for which the generated columns present a smaller width than for the Zone T microstructure to which the deposition of Mg belongs. In our context, this leads to a denser population of thinner columns explaining the evolution of our microstructure in comparison with the metallic samples. This effect is even more pronounced when increasing O_2 , in other words, when the condensing material is close to be fully oxidized. We expect a stabilization of the structure features for higher value of O_2 because the depositing films chemistry is not further modified. It is therefore demonstrated that the presence of even small quantities of O_2 can strongly affects the morphology of the nano-sculpted Mg films.

Because of the morphology of these samples, XPS measurements are much more difficult to perform than for flat surfaces. Therefore, the composition of the porous films has been evaluated by studying the phase constitution using XRD data. Fig. 7 shows the evolution of the XRD patterns for the nano-sculpted samples prepared for $\text{O}_2 = 0, 2.5$ and 5% , respectively. Consistently with the results obtained for the films prepared in conventional geometry, diffraction lines are observed for all samples suggesting that the deposited material is, at least, partly crystallized for all deposition conditions. For the sample prepared for $\text{O}_2 = 0\%$, prepared in the same conditions that reference sample 1, similar diffraction lines can be observed with a preferential growth along the c axis (see Fig. 5 for comparison). In addition, weak hexagonal (112) and (103) MgO lines are observed. This could be explainable by a higher partial oxidation of the film because of its higher surface area in comparison with the reference sample.

Concerning the sample prepared for $\text{O}_2 = 2.5\%$, which is prepared

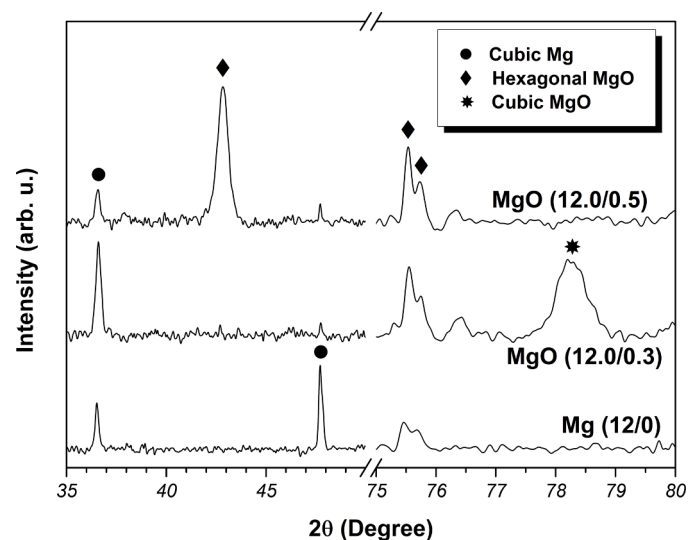


Fig. 7. XRD data of nano-sculpted samples prepared for $\alpha = 85^\circ$ and $P_{\text{tot}} = 0.26$ Pa with $\text{O}_2 = 0\%, 2.5\%$ and 5% , respectively. The sputtering power is 50 W.

for conditions corresponding to the edge of the metal-to-compound transition (on the metallic side), the XRD patterns contains, with similar intensities, cubic Mg lines and a polymorphic mixture of hexagonal and cubic MgO lines. This reveals that this sample is only partially oxidized which is consistent with the fact that the sputtering process is still working in its “metallic mode”. When further increasing O_2 to 5% to reach conditions that correspond to the “compound mode” of the process as determined from conventional geometry experiments, the diffraction spectrum of the sample mostly reveals that the compound is crystallized in its MgO hexagonal phase with, in comparison with reference sample 2, a strong (002) orientation. This could be explained by the utilization of the GLAD geometry considering that the competition between grain growth during the initial growth steps is likely affected by the deposition angle. In addition, it has to be mentioned that, as already observed for reference sample 2, we still observe diffraction peaks related to metallic Mg that seems to be even more important in this case. Again, this could be explained by an impact of the GLAD configuration on the minimum O_2 for which a complete oxidation of the deposited material is reached. Indeed, since the growth mechanism, the surface area of the growing film, the deposition rate and others are dependent on the deposition geometry, it is reasonable to imagine that it could also affect the oxidation rate of the film for a given process condition.

Altogether, this set of data demonstrates the strong impact of oxygen on the MSGD process. It can be concluded from the present work that, in order to optimize the properties of nano-sculpted Mg films for hydrogen storage applications, it is necessary to (i) avoid the presence of any traces of oxygen or water vapor in the deposition chamber and (ii) to protect the as-deposited films by a barrier coating if they have to be vented before the next step of the process.

4. Conclusions

In this work, we provide a clear description of the influence of the presence of oxygen on the chemistry and morphology of nano-sculpted MgO_x thin films prepared by reactive magnetron sputtering in glancing angle configuration. It is shown that, even for non-reactive conditions, a simple exposure of the nano-sculpted films to atmosphere leads to the formation of an oxide/hydroxide layer on the Mg film which could be detrimental for hydrogen storage application. It is therefore necessary to develop protective solution against this oxidation in view of the future utilization of these films.

On the other hand, it is demonstrated that even a slight amount of O₂ in the sputtering gas mixture strongly affects the morphological features of the films by reducing the width of the tilted columns as well as the intercolumnar space by ~50% and even ~60% when considering higher content in oxygen. This is understood by considering the impact of the presence of oxygen on the growth mechanism of the porous columnar films, specifically taking into account the density of initial clusters which is likely higher in the case of reactive conditions.

Author contributions

Conceptualization: **Hui Liang and Rony Snyders**; Methodology: **Hui Liang and Xi Geng**; validation: **Hui Liang, Xi Geng, Adriano Panepinto and Damien Thiry**; Formal analysis: **Hui Liang, Xi Geng and Adriano Panepinto**; Investigation: **Hui Liang and Xi Geng**; Resources: **Hui Liang and Xi Geng**; Data curation: **Hui Liang and Xi Geng**; Writing—original draft: **Hui Liang and Xi Geng**; Writing—review & editing: **Rony Snyders and Wenjiang Li**; Visualization: **Hui Liang**; Supervision: **Rony Snyders and Wenjiang Li**; Project administration: **Rony Snyders, Wenjiang Li and Minfang Chen**; Funding acquisition: **Wenjiang Li and Minfang Chen**.

Declaration of Competing Interest

The authors declare that they have no known competing financial interests or personal relationships that could have appeared to influence the work reported in this paper.

Acknowledgements

This work was supported by F.R.I.A grant of National Fund for Scientific Research (FNRS – Belgium); the Joint Foundation of National Natural Science Foundation of China (Grant No. U1764254), China; 321 Talent project of Nanjing (Grant No. 631783), China; 111 Project (D17003), China.

References

- [1] I. Haas, A. Gedanken, Synthesis of metallic magnesium nanoparticles by sono electrochemistry, *Chem. Commun.* 15 (2008) 1795–1797.
- [2] H.D. Jong, The preparation of carbon-supported magnesium nanoparticles using melt infiltration, *Chem. Mater.* 19 (2007) 6052–6057.
- [3] B.J. Kooi, G. Palasantzas, J.T.M. De Hosson, Gas-phase synthesis of magnesium nanoparticles: a high-resolution transmission electron microscopy study, *Appl. Phys. Lett.* 89 (2006) 267–54.
- [4] M. Momirlan, T.N. Veziroglu, The properties of hydrogen as fuel tomorrow in sustainable energy system for a cleaner planet, *Int. J. Hydrog. Energy* 30 (2005) 795–802.
- [5] M. Aneke, M. Wang, Energy storage technologies and real life applications-A state of the art review, *Appl. Energy* 179 (2016) 350–377.
- [6] S. Basak, K. Shashikala, S.K. Kulshreshtha, Hydrogen absorption characteristics of Zr substituted Ti_{0.85}VFe_{0.15} alloy, *Int. J. Hydrog. Energy* 33 (2008) 350–355.
- [7] M.P. Suh, H.J. Park, T.K. Prasad, D.W. Lim, Hydrogen storage in metal-organic frameworks, *Chem. Rev.* 112 (2012) 782–835.
- [8] W. Li, C. Li, H. M. Magnesium nanowires: enhanced kinetics for hydrogen absorption and desorption, *J. Am. Chem. Soc.* 129 (2007) 6710–6711.
- [9] Y.H. Sun, C.Q. Shen, Q.W. Lai, W.D. Liu, W. Wang, K. Francois, A. Zinsoua, Tailoring magnesium based materials for hydrogen storage through synthesis: current state of the art, *Energy Storage Mater.* 10 (2017) 168–198.
- [10] I.P. Jain, C. Lal, A. Jain, Hydrogen storage in Mg: a most promising material, *Int. J. Hydrog. Energy* 35 (2010) 5133–5144.
- [11] T. Sadhasivam, H.T. Kim, S. Jung, S.H. Roh, J.H. Park, H.Y. Jung, Dimensional effects of nanostructured Mg/MgH₂ for hydrogen storage applications: a review, *Renew. Sustain. Energy Rev.* 72 (2017) 523–534.
- [12] K.J. Jeon, H.R. Moon, A.M. Ruminski, B. Jiang, C. Kisielowski, R. Bardhan, Air-stable magnesium nanocomposites provide rapid and high-capacity hydrogen storage without using heavy-metal catalysts, *Nature Mater.* 4 (2011) 286–290.
- [13] J.G. Yuan, Y.F. Zhu, Y. Li, L.Q. Li, Effect of multi-wall carbon nanotubes supported palladium addition on hydrogen storage properties of magnesium hydride, *Int. J. Hydrog. Energy* 39 (2014) 10184–10194.
- [14] H. Liang, X. Geng, W. Li, A. Panepinto, D. Thiry, M. Chen, R. Snyders, Experimental and modeling study of the fabrication of mg nano-sculpted films by magnetron sputtering combined with glancing angle deposition, *Coatings* 9 (2019) 361.
- [15] H.B. Yao, Y. Li, A.T.S. Wee, An XPS investigation of the oxidation/corrosion of melt-spun Mg, *Appl. Surf. Sci.* 158 (2000) 112–119.
- [16] P. Scherrer, Bestimmung der Größe und der inneren Struktur von Kolloidteilchen mittels Röntgenstrahlen, *Nachr. Ges. Wiss. Göttingen* 26 (1918) 98–100.
- [17] A.M. Ruminski, R. Bardhan, A. Brand, S. Aloni, J.J. Urban, Synergistic enhancement of hydrogen storage and air stability via Mg nanocrystal-polymer interfacial interactions, *Energy Environ. Sci.* 6 (2013) 3267–3271.
- [18] Y. Matsuda, K. Otomo, H. Fujiyama, Quantitative modeling of reactive sputtering process for MgO thin film deposition, *Thin Solid Films* 390 (2001) 59–93.
- [19] D. Depla, J. Heamers, R. De Gryse, Discharge voltage measurements during reactive sputtering of oxides, *Thin Solid Films* 515 (2006) 468–471.
- [20] R. Snyders, J.-P. Dauchot, M. Hecq, Synthesis of metal oxide thin films by reactive magnetron sputtering in Ar/O₂ mixtures: an experimental study of the chemical mechanisms, *Plasm. Process. Polym.* 4 (2007) 113–126.
- [21] D. Milcius, J. Grbović-Novaković, R. Zostautienė, M. Lelis, D. Girdzevicius, M. Urbonavicius, Combined XRD and XPS analysis of ex-situ and in-situ plasma hydrogenated magnetron sputtered Mg films, *J. Alloys Compd.* 647 (2015) 790–796.
- [22] H.B. Yao, Y. Li, A.T.S. Wee, An XPS investigation of the oxidation/corrosion of melt-spun Mg, *Appl. Surf. Sci.* 158 (2000) 112.
- [23] J.C. Fuggle, L.M. Watson, D.J. Fabian, S. Sffrosman, X-ray photoelectron studies of the reaction of clean metals (Mg, Al, Cr, Mn) with oxygen and water vapour, *Surf. Sci.* 49 (1975) 61–76.
- [24] J.F. Moulder, W.F. Stickle, P.E. Sobol, K.D. Bomben, Handbook of X-ray photoelectron spectroscopy, *Phys. Electron.* (1992) 52–53.
- [25] E. Kusano, An investigation of hysteresis effects as a function of pumping speed, sputtering current, and O₂/Ar ratio, in Ti-O₂ reactive sputtering processes, *J. Appl. Phys.* 70 (1991) 7089.
- [26] S. Pétigny, H. Mostéfa-Sba, B. Domenichini, E. Lesniewska, A. Steinbrunn, S. Bourgeois, Superficial defects induced by argon and oxygen bombardments on (110) TiO₂ surfaces, *Surf. Sc.* 410 (1993) 250–257.
- [27] I. Petrov, P.B. Bama, L. Hultman, J.E. Greene, Microstructural evolution during film growth, *J. Vac. Sci. Technol. A* 21 (2003) 117.
- [28] A. Anders, A structure zone diagram including plasma-based deposition and ion etching, *Thin Solid Films* 518 (2010) 4087–4090.